14th International Symposium on Turbulence and Shear Flow Phenomena (TSFP14)
Heidelberg, Germany, July 28–31, 2026

WATER-HAMMER JETTING EMANATING FROM IMPACTING DROPS

Vladimir Bogdanov
Institute of Aerodynamics and Fluid Mechanics
Technical University of Munich
85748 Garching, Germany
vladimir.bogdanov@tum.de

Felix S. Schranner
Engineering Risk Analysis Group
Technical University of Munich
85748 Garching, Germany
schranne@tum.de

ABSTRACT

This work studies the formation and evolution of focused jets. In particular, the dependence of jet formation and evolution on selected physical parameters is investigated. The data are obtained using the conservative sharp-interface method for the setups described in Castillo-Orozco et al. (2015) .

INTRODUCTION

Liquid jets can be observed in a number of natural phenomena. A type of the liquid jets which is of a distinct interest due to its frequent usage in science and industry is a focused liquid jet. To optimally employ focused jets for specific use cases, the parametric dependencies of their formation and evolution must be well understood. A clear understanding of these phenomena requires insight into the physics of jet formation.

Experiments are limited in their capacity as they are often sensitive to the experimental design in an unexpected manner George (1990) and are never free of alleatoric uncertainties. The aforementioned drawbacks of physical experiments lead to the necessity to perform numerical simulations and to thereby specifically model the physics accurately.

However, the study of shear-flow configuration of the highly focused liquid jets with numerical simulations is also challenging. The core - the highly focused jet - is characterized by fine-scaled, quickly evolving structures. The periphery is characterized by a free surface and a bulk liquid, both carrying and refocusing the wave-dynamics such to form a highly focused liquid jet.

These challenges can be tackled with a very-low dissipative gradient-capturing flow solver, proper physical models of the liquid and gaseous phases, a sharp-interface representation and sufficient resolution.

However, when seeking to understand the parametric dependency of the jet formation and evolution, the actual challenge is to conduct a study campaign computationally efficiently. Therefore, computational resources need to be focused without loss of accuracy whenever possible and the axisymmetry of the configuration needs to be exploited. The approach has been proven to be qualitatively and quantitatively accurate for similar applications in a number of jet-formation studies, i.e., Zahoor et al. (2021), Saade et al. (2021), Peters et al. (2013) and Kyriazis et al. (2019).

For these reasons, the simulations are conducted using the level-set based sharp-interface multiresolution solver ALPACA Hoppe et al. (2022). This solver demonstrates its suitability to predict the multiphase-flow behavior in diverse scenarios, e.g., Kaiser et al. (2020); Hoppe et al. (2019); Fleischmann et al. (2019); Bußmann et al. (2023); Winter et al. (2023). The computational efficiency of the method demonstrated in Hoppe et al. (2022) allows to adequately resolve fine scales where essential for the representation of focused liquid jets.

In this work the solver's capability in exploiting the axisymmetry of the shear-flow configuration shall be explored. Note that the challenge therein lies in the fact that the highly-focused jet forms and evolves at the symmetry and not at the outer boundary, posing a challenge in terms of accuracy and robustness on a numerical solver.

The work is structured as follows: the physical model, numerical implementation, and numerical setup are described, followed by presentation and discussion of simulation results from a series of parametric studies.

PHYSICAL MODEL AND ITS NUMERICAL IMPLEMENTATION

Physical model

The compressible Navier-Stokes equations, including viscous, surface-tension effects and gravitational acceleration, hold:

$$\frac{\partial \mathbf{U}}{\partial t} + \nabla \mathbf{F}(\mathbf{U}) = \mathbf{S}, \tag{1}$$

where $\mathbf{U} = (\rho, \rho \mathrm{u}_1, \rho \mathrm{u}_2, \rho \mathrm{u}_3, \rho \mathrm{e}_\mathrm{t})^\mathrm{T}$ is the vector of conservatives, $\mathbf{F} = (\rho \mathbf{u}, \rho \mathbf{u} \otimes \mathbf{u} - \mathbf{\Pi}, \rho \mathrm{e}_\mathrm{t} \mathbf{u} - \mathbf{u} \cdot \mathbf{\Pi})^\mathrm{T}$ is the vector of fluxes and $\mathbf{S} = \left(0, \rho \mathbf{g}, \rho \mathbf{g}^\mathrm{T} \cdot \mathbf{u}\right)$ is the vector of source terms. In this case, ρ is the non-dimensional density, $\mathbf{u}$ is the non-dimensional velocity, $\mathbf{\Pi}$ is the non-dimensional stress tensor, e_t is the non-dimensional specific total energy, p is the static, non-dimensional pressure. The non-dimensionalization is described in detail in Hoppe et al. (2022).

The set of equations is closed with the Tait equation of state for the liquid phase:

$$p = p(\rho) = p_1 \left[\left(\frac{\rho}{\rho_0} \right)^{\omega} - 1 \right] + p_0, \tag{2}$$

where ω is the heat capacity ratio, ρ_0 is the reference density, p_0 is the reference pressure.

For the gaseous phase, the ideal-gas equation of state holds:

$$p = (\omega - 1)\rho e \tag{3}$$

Numerical implementation

A finite-volume approach on a Cartesian grid is applied to solve Eq. 1.

The two phases and the interface are treated by a sharp-interface method, see e.g. Schranner (2017); Schranner & Adams (2016); Schranner et al. (2016). For the time integration, the 3rd-order Runge-Kutta TVD scheme Gottlieb & Shu (1998) is utilized. An adaptive multi-resolution approach Harten (1994) is used to increase the computational efficiency.

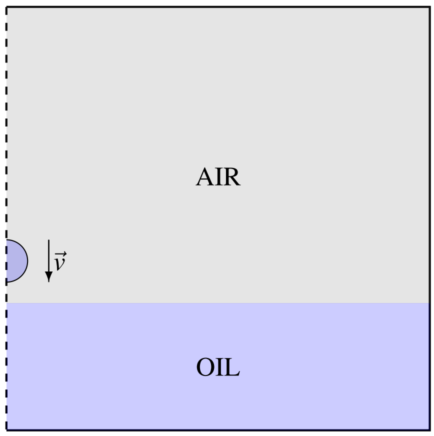

Figure 1. Initial setup.

Numerical setup

The numerical setup is designed to replicate the initial conditions of experiments from Castillo-Orozco et al. (2015). A rectangular domain is filled with air and silicone oil, see Fig. 1, so that a small drop of silicone oil surrounded by air is falling into a pool of silicone oil. The symmetry boundary condition is applied at the left domain boundary. The right and bottom boundaries are solid walls, and the top boundary uses a zero-gradient boundary condition. The simulation is run axisymmetrically. The gravitational acceleration is directed downwards.

The air and oil, except for the drop, are initially static.

RESULTS AND DISCUSSION

Verification

To demonstrate that ALPACA adequately captures the physical behavior of the liquid jet in a weakly-compressible framework and to justify the resolution chosen for the subsequent numerical experiments, the simulations using the earlier introduced setup have been performed with effective resolutions of 1024 × 1024, 2048 × 2048, and 4096 × 4096 cells on the finest level. Fig. 2 depicts the shift of the jet tip as a function of time for the three simulations. While the results for the coarsest resolution diverges from the other time-evolutions shortly after $t = 0.02$, the trends of h for the two finest resolutions remain nearly identical until the jet reaches its peak. This justifies the choice of 2048 × 2048 cells for the subsequent simulations, as the maximum jet tip height is used as the key variable for the sensitivity analysis in the following sections.

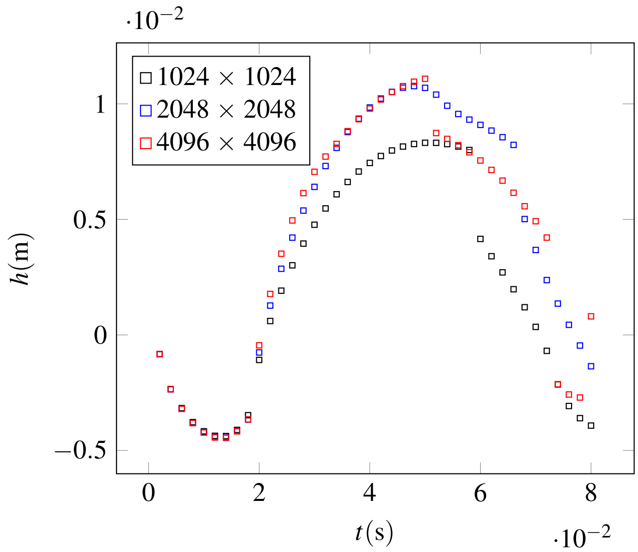

Figure 2. Jet-tip height h as a function of time at different effective resolutions

Effect of the surface tension

The effect of the following independent quantities is studied: surface tension, viscosity, initial velocity of the drop, and gravitational acceleration. This choice is based on the significant influence each of quantity has on jet behavior: surface tension and viscosity represent fluid properties, initial velocity characterizes the fluid state at the initial moment, and gravitational acceleration characterizes the external conditions.

This subsection focuses on surface tension. Figures 3 and 4 show the jet-tip height as a function of time, with results grouped by parameter value in ascending order for clarity (this grouping convention is used throughout this and the following subsections). From Figure 3, it is visible that the surface-tension coefficient starts to play a noticeable role in the jet evolution starting from the values around $\sigma = 10$ mN/m. For $\sigma = 10$ mN/m and $\sigma = 15$ mN/m, the formation of secondary droplets is observed, which are represented by the discontinuities of the function $h = h(t)$. However, with further increase of the surface tension coefficient, the tendency for the secondary droplet formation declines, as clearly visible in Figure 4.

Effect of the viscosity

Dynamic viscosity is another liquid parameter with a strong impact on jet behavior. As expected, the fastest jet formation occurs at the lowest viscosities (see Figure 5). For

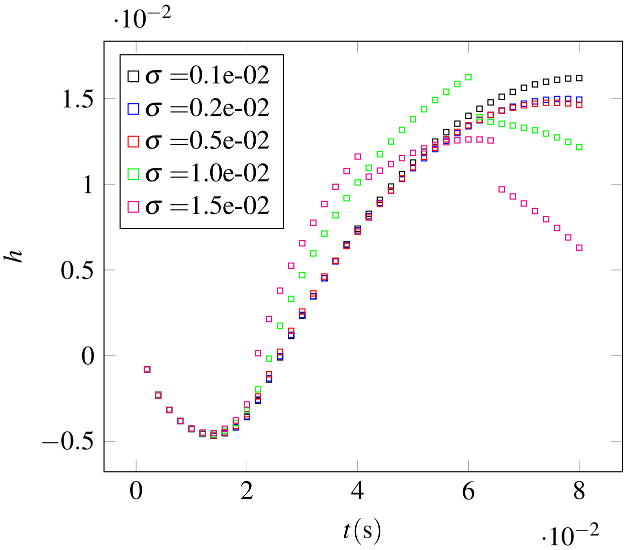

Figure 3. $h = h(t)$ for different surface-tension coefficients (lower values)

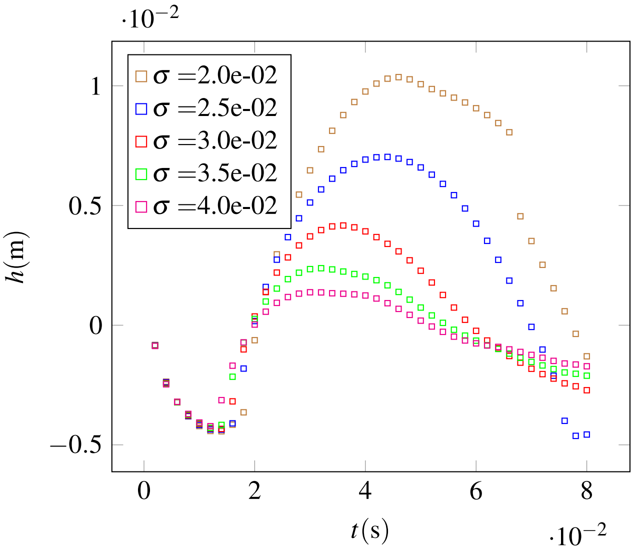

Figure 4. $h = h(t)$ for different surface-tension coefficient (higher values)

most simulations in this subsection, the behavior follows this sequence: the jet forms and reaches its maximum height, the first secondary droplet forms, the main jet descends, and in some cases, a second secondary droplet forms (see the results for $\mu = 0.0035$ kg/ms, Figure 6, as an example). However, for $\mu = 0.003$ kg/ms, the secondary droplet does not form at the maximum height but only near the end of the simulation. The evolution profiles are nearly identical up to $t = 20$ ms. Afterwards jets with the lowest viscosities exhibit the most rapid growth to peak height. The secondary droplets form for all viscosities, earliest at $t \approx 40$ ms ($\mu = 0.0055$ kg/ms, Figure 7), latest at $t \approx 80$ ms ($\mu = 0.003$ kg/ms, Figure 5).

Effect of the initial velocity

Initial velocity, as a characteristic of the drop's initial-state, has a major impact on jet behavior. This impact is especially pronounced at lower velocities, as shown in Figure 8. At the lowest velocity $v = 1.0$ m/s, the jet development is

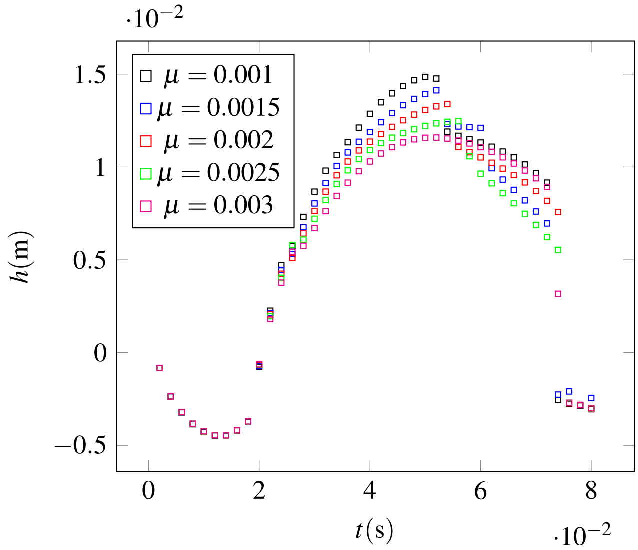

Figure 5. $h = h(t)$ for different dynamic viscosities (lower values)

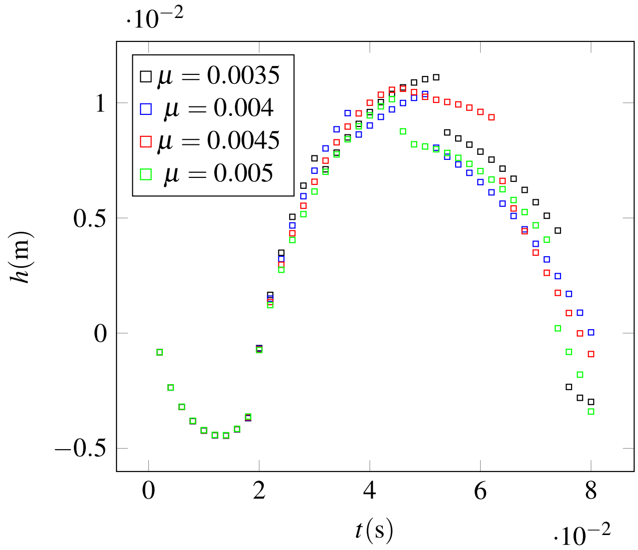

Figure 6. $h = h(t)$ for different dynamic viscosities (middle values)

not characterized by secondary droplet formation. However, at higher velocities, the maximum height increases and one or two consecutive secondary droplets typically form. Notably, for velocities above $v = 3.0$ m/s (Figure 9), further velocity increases have less influence on jet behavior compared to the pronounced changes observed for similar velocity increments at lower velocities.

Effect of the gravitational acceleration

To examine the influence of external conditions on jet formation, simulations with different gravitational accelerations have been conducted. Similar to the sensitivity to initial velocity observed in the initial-velocity parametric study, early jet development shows high sensitivity to gravity until reaching maximum height (Figure 10) but is much less sensitive at higher values (Figure 11). Moreover, at the largest values, a second jet begins to form after the initial jet subsides, with the effect being especially strong for $g = 45.0$ m/s^2.

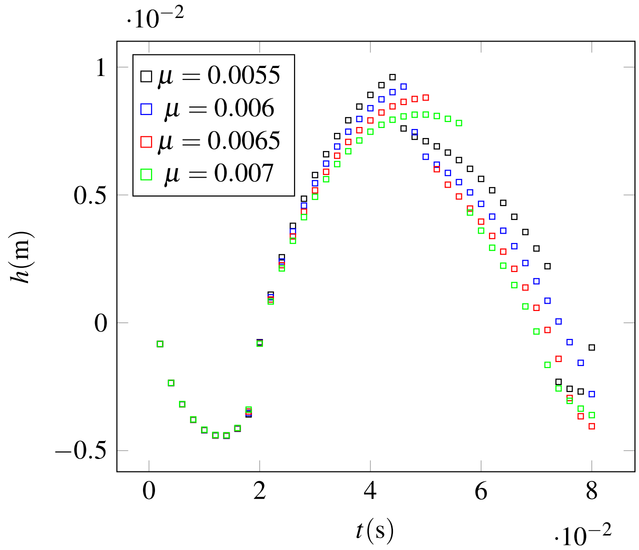

Figure 7. $h = h(t)$ for different dynamic viscosities (higher values)

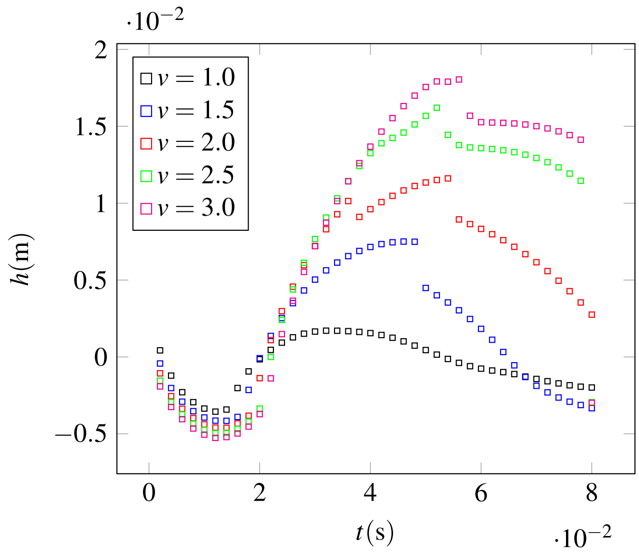

Figure 8. $h = h(t)$ for different velocities (lower values)

DISCUSSION AND CONCLUSION

The following evolution stages are typically observed for the jets investigated in this work: (1) impact cavity formation; (2) jet growth to maximum height; (3) secondary droplet formation; (4) jet decline sometimes accompanied by additional secondary droplet formation. Our results for jet evolution are qualitatively consistent with the ones obtained by Castillo-Orozco et al. (2015). This demonstrates the capability of the numerical simulations obtained using the conservative sharp-interface method to adequately represent the behavior of a drop-triggered liquid jet, including the formation of the secondary drops.

The parametric studies presented in this work capture the dependence of the jet-profile evolution on particular characteristics of the fluids, the ambient conditions and the initial setup. The evolution characteristics affected involve the speed of the jet formation, the moments of reaching the peak and drop formation and whether the secondary drops are formed at all. Quantifying the influence of individual parameters on specific evolution characteristics remains a subject for future

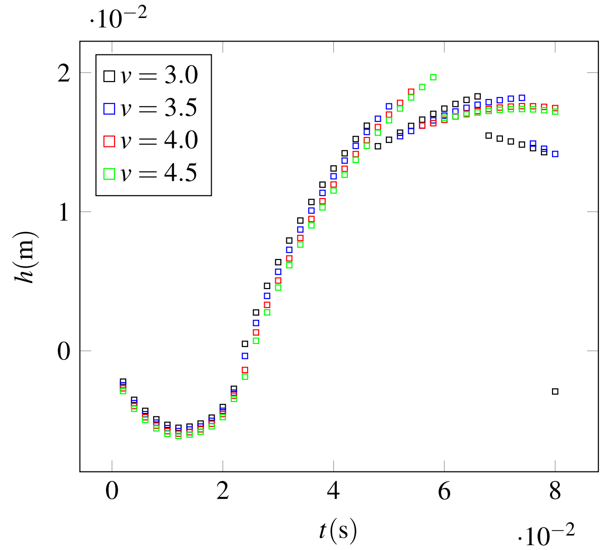

Figure 9. $h = h(t)$ for different velocities (higher values)

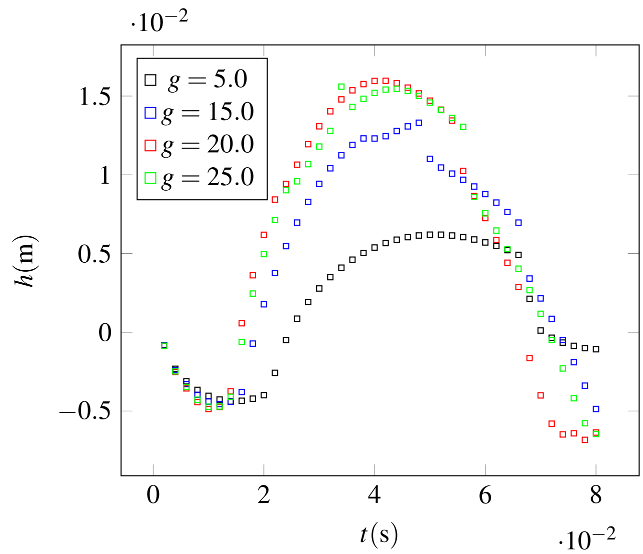

Figure 10. $h = h(t)$ for different gravitational accelerations (lower values)

investigation.

ACKNOWLEDGEMENTS

The authors express their gratitude for the support of Gauss Centre for Supercomputing e.V. via providing computing time on the GCS Supercomputer SuperMUC at Leibniz Supercomputing Centre. V. Bogdanov is a member of the TUM Graduate School.

REFERENCES

Bußmann, Alexander, Riahi, Farbod, Gökce, Bilal, Adami, Stefan, Barcikowski, Stephan & Adams, Nikolaus A. 2023 Investigation of cavitation bubble dynamics near a solid wall by high-resolution numerical simulation. Physics of Fluids **35** (1), 16115.

Castillo-Orozco, Eduardo, Davanlou, Ashkan, Choudhury, Pretam K. & Kumar, Ranganathan 2015 Droplet impact on deep liquid pools: Rayleigh jet to formation of secondary

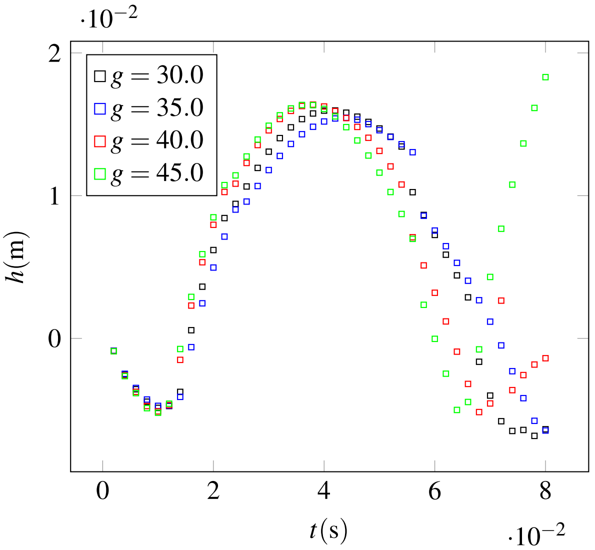

Figure 11. $h = h(t)$ for different gravitational accelerations (higher values)

droplets. Physical Review E - Statistical, Nonlinear, and Soft Matter Physics **92** (5), 053022.

Coleman & Steele 2009 Wiley: Experimentation, Validation, and Uncertainty Analysis for Engineers, 3rd Edition - Hugh W. Coleman, W. Glenn Steele p. 336.

Fleischmann, Nico, Adami, Stefan & Adams, Nikolaus A. 2019 Numerical Symmetry-Preserving Techniques for Low-Dissipation Shock-Capturing Schemes. Computers & Fluids **189**, 94–107.

George, William K. 1990 Governing equations, experiments, and the experimentalist. Experimental Thermal and Fluid Science **3** (6), 557–566.

Gottlieb, Sigal & Shu, Chi-Wang 1998 Total variation diminishing Runge-Kutta schemes. Mathematics of computation of the American Mathematical Society **67** (221), 73–85.

Harten, Ami 1994 Adaptive Multiresolution Schemes for Shock Computations. Journal of Computational Physics **115**, 319–338.

Hoppe, Nils, Pasichnyk, Igor, Allalen, Momme, Adami, Stefan & Adams, Nikolaus A. 2019 Node-Level optimization of a 3D Block-Based Multiresolution Compressible Flow Solver with Emphasis on Performance Portability. In 2019 International Conference on High Performance Computing & Simulation (HPCS), pp. 732–740. IEEE.

Hoppe, Nils, Winter, Josef M., Adami, Stefan & Adams, Nikolaus A. 2022 ALPACA - a level-set based sharp-interface multiresolution solver for conservation laws. Computer Physics Communications **272**, 108246.

Kaiser, J. W.J., Winter, J. M., Adami, S. & Adams, N. A. 2020 Investigation of interface deformation dynamics during high-Weber number cylindrical droplet breakup. International Journal of Multiphase Flow **132**.

Kyriazis, Nikolaos, Koukouvinis, Phoevos & Gavaises, Manolis 2019 Numerical investigations on bubble-induced jetting and shock wave focusing: application on a needle-free injection. Proceedings of the Royal Society A: Mathematical, Physical and Engineering Sciences **475** (2222), 20180548.

Peters, Ivo R, Tagawa, Yoshiyuki, Oudalov, Nikolai, Sun, Chao, Prosperetti, Andrea, Lohse, Detlef & van der Meer, Devaraj 2013 Highly focused supersonic microjets: numerical simulations. Journal of Fluid Mechanics **719**, 587–605.

Saade, Youssef, Jalaal, Maziyar, Prosperetti, Andrea, Lohse, Detlef, Saade, Y, Jalaal, M, Prosperetti, A & Lohse, D 2021 Crown formation from a cavitating bubble close to a free surface. Journal of Fluid Mechanics **926**, 5.

Schranner, F.S., Rozov, V. & Adams, N.A. 2016 Optimization of an implicit large-eddy simulation method for underresolved incompressible flow simulations. AIAA Journal **54** (5).

Schranner, Felix Sebastian 2017 Weakly Compressible Models for Complex Flows. Phd thesis, Technical University of Munich.

Schranner, F S & Adams, N A 2016 A conservative interface-interaction model with insoluble surfactant. Journal of Computational Physics **327**.

Winter, J. M., Abaidi, R., Kaiser, J. W.J., Adami, S. & Adams, N. A. 2023 Multi-fidelity Bayesian optimization to solve the inverse Stefan problem. Computer Methods in Applied Mechanics and Engineering **410**, 115946.

Zahoor, Rizwan, Knoška, Juraj, Bajt, Saša & Šarler, Božidar 2021 Experimental and Numerical Investigation of Gas-Focused Liquid Micro-Jet Velocity. International Journal of Multiphase Flow **135**, 103530.